Unsupervised learning-based interaction force model for non-spherical particles in incompressible flows

FOA: DE-FOA-0002193

Award Number: GRANT13034158

L.-S. Fan (PI)

and

Jianhua Pan and Soohwan Hwang

Department of Chemical and Biomolecular Engineering

The Ohio State University

2020-2023

Outlines

- Introduction
- Objectives
- Pathways
  - Particle Resolved (PR)-DNS and non-spherical particle generation;
  - Geometrical feature extraction (With Auto-encoder (AE));
  - Regression for the force. (With multi-layer perceptron (MLP)).
- Conclusions

1. Introduction

Drag force models for gas-solid flow systems with spherical particles.

- Direct Numerical Simulation;
  - Yu, Z.; Fan, L.-S.; "An Interaction Potential Based Lattice Boltzmann Methods with Adaptive Mesh Refinement (AMR) for Two –Phase Flow Simulation", Journal of Computational Physics, 228, 6456-6478 (2009)
  - Zhou, Q.; Fan, L.-S.; "Direct Numerical Simulation of Low-Reynolds-Number Flow Past Arrays of Rotating Spheres," Journal of Fluid Mechanics 765, 396-423, (2015)
  - Zhou, Q.; Fan, L.-S.; "A second-order accurate immersed boundary-lattice Boltzmann method for particle-laden flows," Journal of computational physics, 268 269-301 (2014)
- Experiments;
- Machine learning.

❖ Different volume fraction;
❖ Wide range for Reynolds number;
❖ Neighboring effects.

Regression Model: Yan, S., He, Y., Tang, T. and Wang, T., 2019. Drag coefficient prediction for non-spherical particles in dense gas–solid two-phase flow using artificial neural network. Powder Technology, 354, pp.115-124.

GAN (Generative adversarial network) to reconstruct the flow field around particles. *Siddani, B., Balachandar, S., Moore, W.C., Yang, Y. and Fang, R., 2020. Machine Learning for Physics-Informed Generation of Dispersed Multiphase Flow Using Generative Adversarial Networks. arXiv preprint arXiv:2005.05363.*

For non-spherical particles

- Difficult to define the geometrical factors
  - sphericity, flatness, elongation and circularity, etc.
- Data for the interaction force between non-spherical particles and the fluids are limited.
  - Analytical solution for sphere, cube, cylinder and disk;
  - Most data are collected from experiments.
- Correlation may be highly-nonlinearity.

2. Objective of the projects

- Developing a neural network-based force model:
  - For a diversity of non-spherical particles;
  - From low O(1) to moderate O(100) Reynolds number;
  - From low to high volume fraction,
  - For both fixed bed and fluidized (Stokes number effect) bed.

3. Pathways.

1. Data generation using PR-DNS method to explore the parameter spaces [geometrical (shape factor) and physical (e.g., viscosity and density) spaces]
2. Variational auto-encoder (VAE) will be utilized to extract the primitive geometrical factors of a non-spherical particles.
3. A multi-layer perceptron (MLP) will then be supplied as a regressor for both the drag and lifting force of the non-spherical particles.
4. Linking to MFiX.

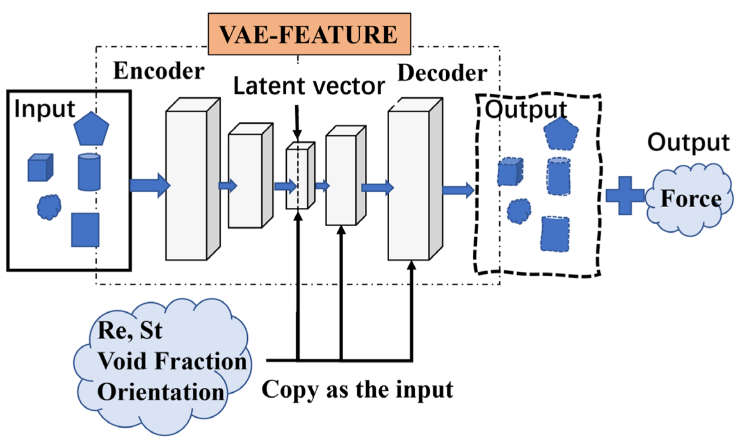

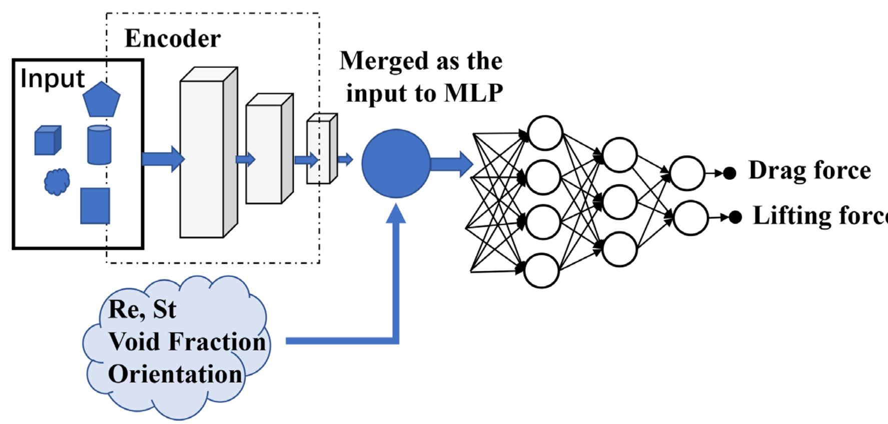

PR-DNS Simulation Technique

Technique	Advantage	Disadvantage
Body-fitted mesh	Accurate at the particle boundaries.	Fixed particle with prescribed shape. Difficult to generate high quality mesh for complicated geometries.
Immersed boundary method.	Cartesian Grids. Easy to handle complicated geometries.	Accuracy near particle boundaries decreased; Redundant grids far from boundaries due to uniform grids.

Discontinous Galerkin Spectral Element method (DGSEM) (Compact support)

GKS scheme (Low storage than LBM)

+

Adaptive mesh refine (AMR)	Highly decrease the redundant grids far from boundaries; Improve the efficiency of simulation.

GKS scheme

- Gas kinetic theory
  - *f(x,v,t):* particle ("molecule") distribution function
  - PDF changes through particle propagation/collision
- Boltzmann equation:

$$\frac{\partial f(\mathbf{x},\mathbf{v},t)}{\partial t} + \mathbf{v}\cdot\nabla_x f = Q$$

BGK collision scheme

$$Q = -\frac{f(\mathbf{x},\mathbf{v},t) - g(\mathbf{x},\mathbf{v},t)}{\tau}$$

- GKS

$$\int \frac{\partial f(\mathbf{x},\mathbf{v},t)}{\partial t}\Xi\, d\mathbf{v} + \int \mathbf{v}\cdot\nabla_x f\,\Xi\, d\vec{v} = \int Q\Xi\, d\mathbf{v}, \quad \Xi = (1,\mathbf{v})^T$$

$$\Rightarrow \quad \frac{\partial \rho}{\partial t} + \nabla_x F_1 = 0, \quad \frac{\partial \rho u_1}{\partial t} + \nabla_x F_2 = 0,$$
$$\frac{\partial \rho u_2}{\partial t} + \nabla_x F_3 = 0, \quad \frac{\partial \rho u_3}{\partial t} + \nabla_x F_4 = 0$$

$$g(\rho,\mathbf{v}) = \begin{cases} \dfrac{\rho}{4\pi} & if\,(\mathbf{v}-\mathbf{u})^2 = c^2 \\ 0 & otherwise \end{cases}$$

$$\mathbf{u} = (u_1, u_2, u_3)$$

$$f\ (\mathbf{x}\ ,\mathbf{v}\ ,t) = \frac{1}{\tau}\int_{t_0}^{t} g(\mathbf{x}-\mathbf{v}(t-t'),t',\mathbf{v})e^{-(t-t')/\tau}dt' + e^{-(t-t_0)/\tau} f_0(\mathbf{x}-\mathbf{v}(t-t_0),t_0,\mathbf{v})$$

Two scales in GKS

Mesoscopic (velocity distribution function)

Macroscopic (continuous fluid)

Variables:

PDF: *f(x,t)*

Relaxation time: τ

Density: $\rho = \int f \, d\mathbf{v}$

Momentum: $\rho \mathbf{u} = \int f \, \mathbf{v} \, d\mathbf{v}$

Viscosity: $\nu = \tau c^2 / D$

Equations:

$$\frac{\partial f(\vec{x}, \vec{v}, t)}{\partial t} + \vec{v} \cdot \nabla_x f = Q$$

Boltzmann Equation

$$\frac{\partial \rho}{\partial t} + \nabla \cdot (\rho \mathbf{u}) = 0$$

$$\frac{\partial \mathbf{u}}{\partial t} + \mathbf{u} \cdot \nabla \mathbf{u} = -\frac{1}{\rho} \nabla p + \nu \nabla^2 \mathbf{u}$$

Continuity & Navier-Stokes

Ma<<O(1)
Chapman-Enskog expansion

$p = \rho c^2 / D$

Constructing *GKS flux*

$$g(\rho, \mathbf{v}) = \begin{cases} \dfrac{\rho}{4\pi} & if\ (\mathbf{v}-\mathbf{u})^2 = c^2 \\ 0 & otherwise \end{cases}$$

- For spherical function-based equilibrium distribution

$$\int g(0,t)\mathbf{v}\ \Xi d\mathbf{v} = \int_0^{2\pi}\int_0^{\pi} \frac{\rho}{4\pi} \boldsymbol{\xi}\Xi d\varphi d\theta$$

$$\xi_1 = u_1 + c\sin\varphi\cos\theta$$
$$\xi_2 = u_2 + c\sin\varphi\sin\theta$$
$$\xi_3 = u_3 + c\cos\varphi$$

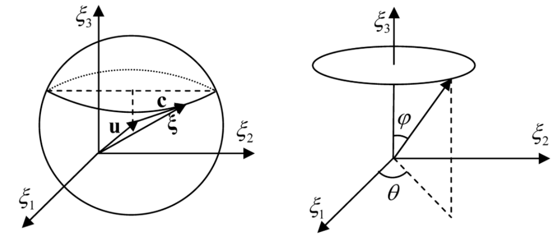

$$\begin{aligned} f(0,t) &= f^{eq}(0,t) + f^{neq}(0,t) \\ &= g(0,t) - \tau\left(\frac{\partial g}{\partial t} + \mathbf{v}\cdot\nabla g\right) \\ &= g(0,t) + \frac{\tau}{\delta t}\left(g(-\mathbf{v}\delta t, t-\delta t) - g(0,t)\right) + O(\delta t^2) \end{aligned}$$

$$\begin{aligned} F &= \int f(0,t)\mathbf{v}\Xi d\mathbf{v} \\ &\approx \int g(0,t)\mathbf{v}\Xi d\mathbf{v} + \frac{\tau}{\delta t}\left(\int g(-\mathbf{v}\delta t, t-\delta t)\mathbf{v}\Xi d\mathbf{v} - \int g(0,t)\mathbf{v}\Xi d\mathbf{v}\right) \\ &= \int_0^{2\pi}\int_0^{\pi} \frac{\rho^{face}}{4\pi}\boldsymbol{\xi}^{face}\Xi^{face} d\varphi d\theta + \frac{\tau}{\delta t}\left(\int_0^{2\pi}\int_0^{\pi} \frac{\rho^{sph}}{4\pi}\boldsymbol{\xi}^{sph}\Xi^{sph} d\varphi d\theta - \int_0^{2\pi}\int_0^{\pi} \frac{\rho^{face}}{4\pi}\boldsymbol{\xi}^{face}\Xi^{face} d\varphi d\theta\right) \\ &= F^I + \frac{\tau}{\delta t}(F^{II} - F^I) \end{aligned}$$

Constructing *GKS flux*

- Through compatibility equation

$$W^{face} = \int g(0,t)\Xi d\mathbf{v} = \int g(-\mathbf{v}\delta t, t-\delta t)\Xi d\mathbf{v} =$$

$$= \left(\int_0^{2\pi}\int_0^{\pi} \frac{\rho^{sph,L}}{4\pi} \xi^{sph,L} \Xi^{sph,L} d\varphi d\theta \,|\, \xi_1^{face} > 0 \right)$$

$$+ \left(\int_0^{2\pi}\int_0^{\pi} \frac{\rho^{sph,R}}{4\pi} \xi^{sph,R} \Xi^{sph,R} d\varphi d\theta \,|\, \xi_1^{face} < 0 \right)$$

$$F^{II} = \left(\int_0^{2\pi}\int_0^{\pi} \frac{\rho^{sph,L}}{4\pi} \xi^{sph,L} \Xi^{sph,L} \xi_1^{sph,L} d\varphi d\theta \,|\, \xi_1^{face} > 0 \right)$$

$$+ \left(\int_0^{2\pi}\int_0^{\pi} \frac{\rho^{sph,R}}{4\pi} \xi^{sph,R} \Xi^{sph,R} \xi_1^{sph,R} d\varphi d\theta \,|\, \xi_1^{face} < 0 \right)$$

$$W^{face} = \left[\left(\rho, \rho u_1, \rho u_2, \rho u_3 \right)^{face} \right]^T$$

$$\Downarrow$$

Inviscid Flux F^I

$$\xi^{sph,L}, \xi^{sph,R}, \xi^{face}, \rho^{sph,L}, \rho^{sph,R}, \rho^{face}$$

Can be determined by the reconstructed value of the conserved variables, i.e., $\rho, \rho u_1, \rho u_2, \rho u_3$

Second order DGSEM+GKS

Solutions are represented by cell-wise continuous polynomials

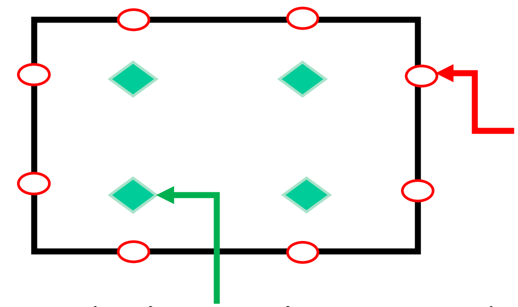

$$\frac{\partial W}{\partial t} + \nabla \bullet F = 0,$$

$$W = \sum_N W_i \phi_i$$

ϕ_i are Lagrangian polynomials for each solution point

$$\int_\Omega \phi_j \frac{\partial \sum_N W_i \phi_i}{\partial t} d\Omega + \int_\Omega \nabla \bullet (\mathbf{F} \phi_j) d\Omega - \int_\Omega \mathbf{F} \bullet \nabla(\phi_j) d\Omega = 0,$$

$$\int_\Omega \phi_j \frac{\partial \sum_N W_i \phi_i}{\partial t} d\Omega + \boxed{\int_{\partial\Omega} (\mathbf{F} \phi_j) \mathbf{n} dS} - \boxed{\int_\Omega \mathbf{F} \bullet \nabla(\phi_j) d\Omega} = 0,$$

Calculated by the conserved variables and their gradients at the interface

Why DGSEM?

1.Compact support

Avoid the reconstruction matrix or ghost cells in adaptive mesh refinement.

2. Efficiency in volume and face integration.

Immersed boundary method

Direct forcing schemes with diffusion delta function.

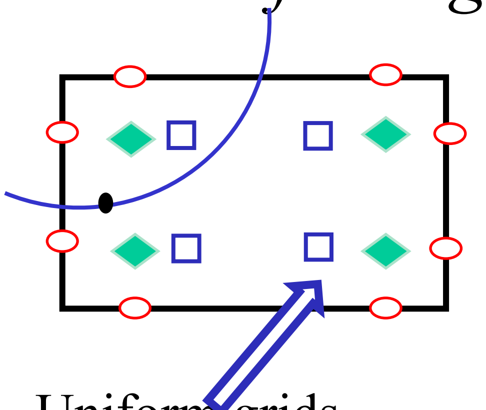

Uniform grids

Prediction step without Lagrangian marker force

$$\frac{\rho_i^{\,*} - \rho_i^{\,n}}{\Delta t} = rhs^1{}_i, \quad \frac{\rho u_{1i}^{\,*} - \rho u_{1i}^{\,n}}{\Delta t} = rhs^2{}_i$$

$$\frac{\rho u_{2i}^{\,*} - \rho u_{2i}^{\,n}}{\Delta t} = rhs^3{}_i, \quad \frac{\rho u_{3i}^{\,*} - \rho u_{3i}^{\,n}}{\Delta t} = rhs^4{}_i$$

$$\mathbf{u}^{n+1}(x), \rho^{n+1}(x)$$

Interpolate the solution to the uniform grid points inside the spectral element.

Interpolate back to the solution points inside the spectral element.

$$\tilde{\mathbf{u}}(x), \tilde{\rho}(x)$$

$$\mathbf{U}(s) = \sum \tilde{\mathbf{u}}(x)\delta(x-s)\Delta h^3$$

$$\Upsilon(s) = \sum \tilde{\rho}(x)\delta(x-s)\Delta h^3$$

$$F(s) = \frac{\Upsilon(s)U^{Lag} - \Upsilon(s)\mathbf{U}(s)}{\Delta t}$$

$$f(x) = \sum F(s)\delta(x-s)ds\Delta h^3$$

$$\tilde{u}(x) = \tilde{u}(x) + f(x)\Delta t$$

Iteration

Adaptive mesh refinement

- **Adaptive Mesh Refinement for particle simulations**
  - Solid boundaries: boundary layer, critical to flow field;
  - AMR: Locally refined, automatic adjustment;
  - For simulation of dilute solids, the efficiency could be greatly improved.

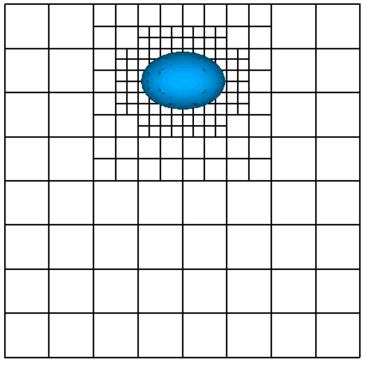

- Mesh generation and management:
  - Block structured Cartesian mesh *Paramesh (Olson, 2006)*
  - Oct-tree based refinement, p4est (Carsten Burstedde, etc.,)

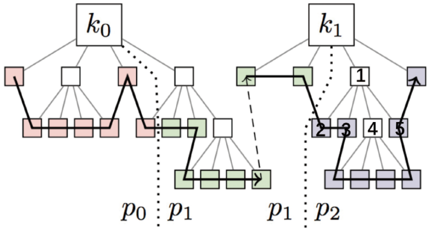

More flexible and finer grained of adaptivity.

AMR of LBM method

- On coarse/fine boundary
  - Coarse to fine: *explode*
  - Fine to coarse: *coalesce*

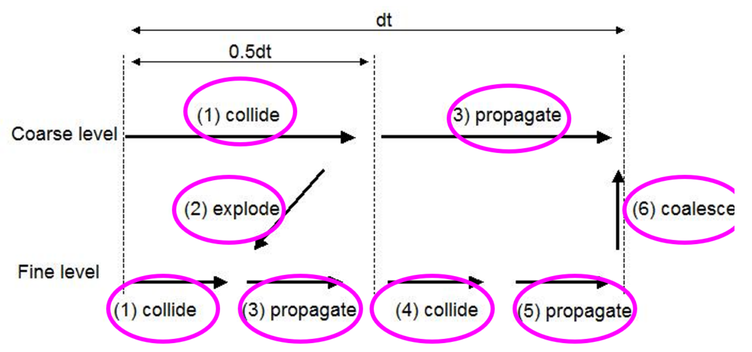

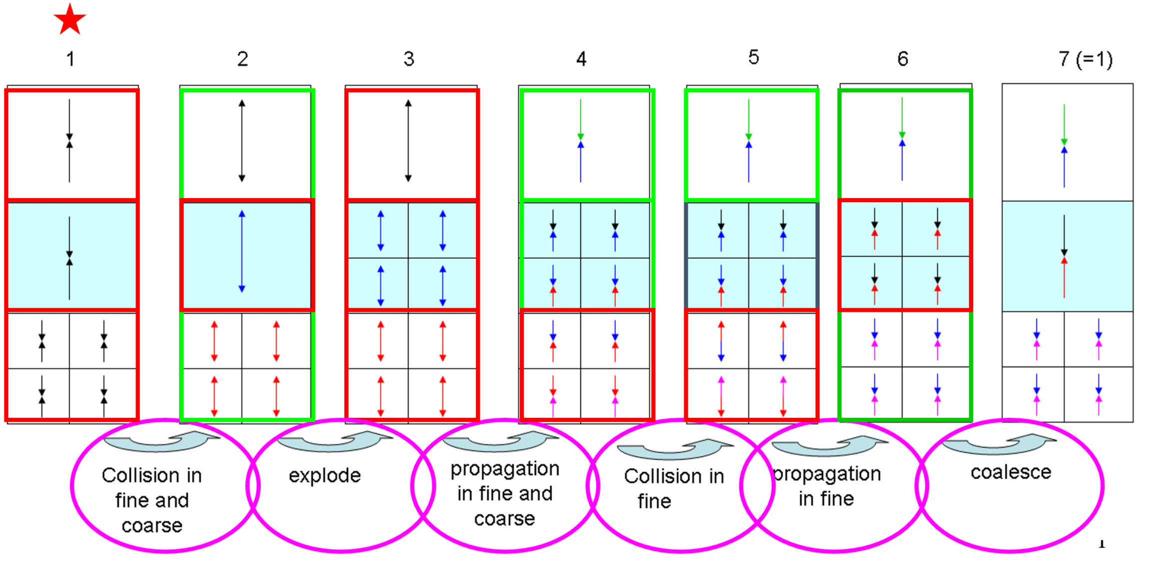

Yu, Z.; Fan, L.-S.; "An Interaction Potential Based Lattice Boltzmann Methods with Adaptive Mesh Refinement (AMR) for Two –Phase Flow Simulation", Journal of Computational Physics, 228, 6456-6478 (2009)

AMR of DGSEM-GKS

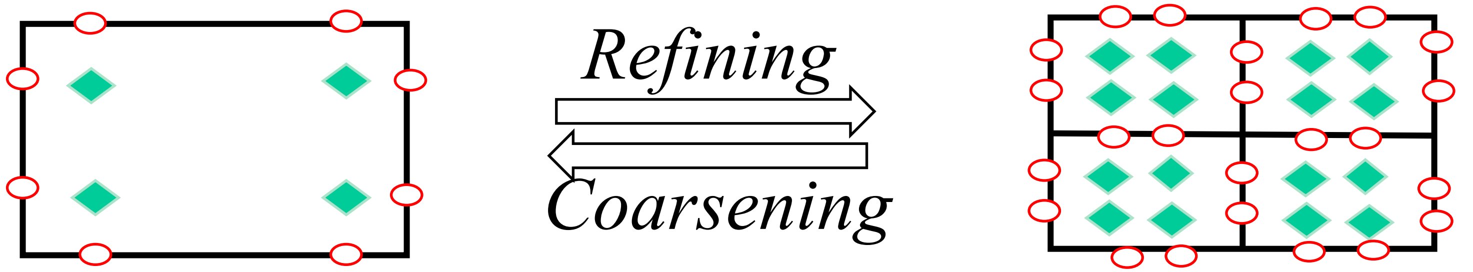

- Unlike the LBM method in AMR, all the elements can be time-forward simultaneously.
- Mesh around the particle boundaries will always be kept in the finest level.

Preliminary results

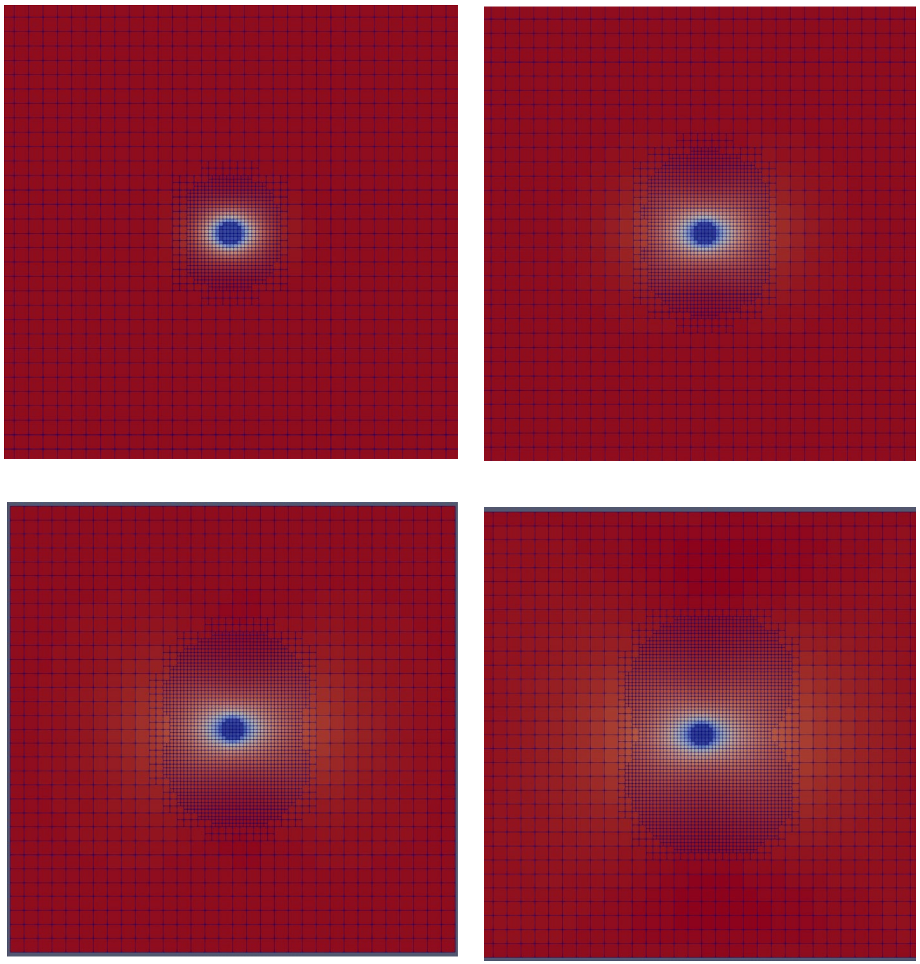

- *3D, Re=0.2, Particle diameter is 6 Δh*
- *Computational domain size is 128 Δh*

$N\colon N_{uniform}$= 1:22.4

Velocity magnitude

Non-spherical particle generation

Spherical Harmonics method

$$\begin{pmatrix} x(\theta,\phi) \\ y(\theta,\phi) \\ z(\theta,\phi) \end{pmatrix} = \begin{pmatrix} \sum_{l=0}^{l_{\max}} \sum_{m=-l}^{l} c_{x,l}^{m} Y_l^m(\theta,\phi) \\ \sum_{l=0}^{l_{\max}} \sum_{m=-l}^{l} c_{y,l}^{m} Y_l^m(\theta,\phi) \\ \sum_{l=0}^{l_{\max}} \sum_{m=-l}^{l} c_{z,l}^{m} Y_l^m(\theta,\phi) \end{pmatrix} \qquad \mathbf{C}_1 = -\sqrt{\frac{\pi}{6}} \begin{pmatrix} -1 & 0 & 1 \\ EI \times i & 0 & EI \times i \\ 0 & \sqrt{2}EI \times FI & 0 \end{pmatrix}$$

x, y, z (θ, φ) : The Cartesian coordinates of a vertex.

$\theta \in [0,\pi]$ and $\phi \in [0,2\pi]$

$Y_l^m(\theta, \varphi)$: Spherical harmonics of degree l and order m.

Orthogonal basis to represent the spherical surface

C_l^m : Randomized spherical harmonics coefficients of degree l and order m.

Normalized with spherical descriptor, d_l

EI : Elongation index, FI : Flatness index

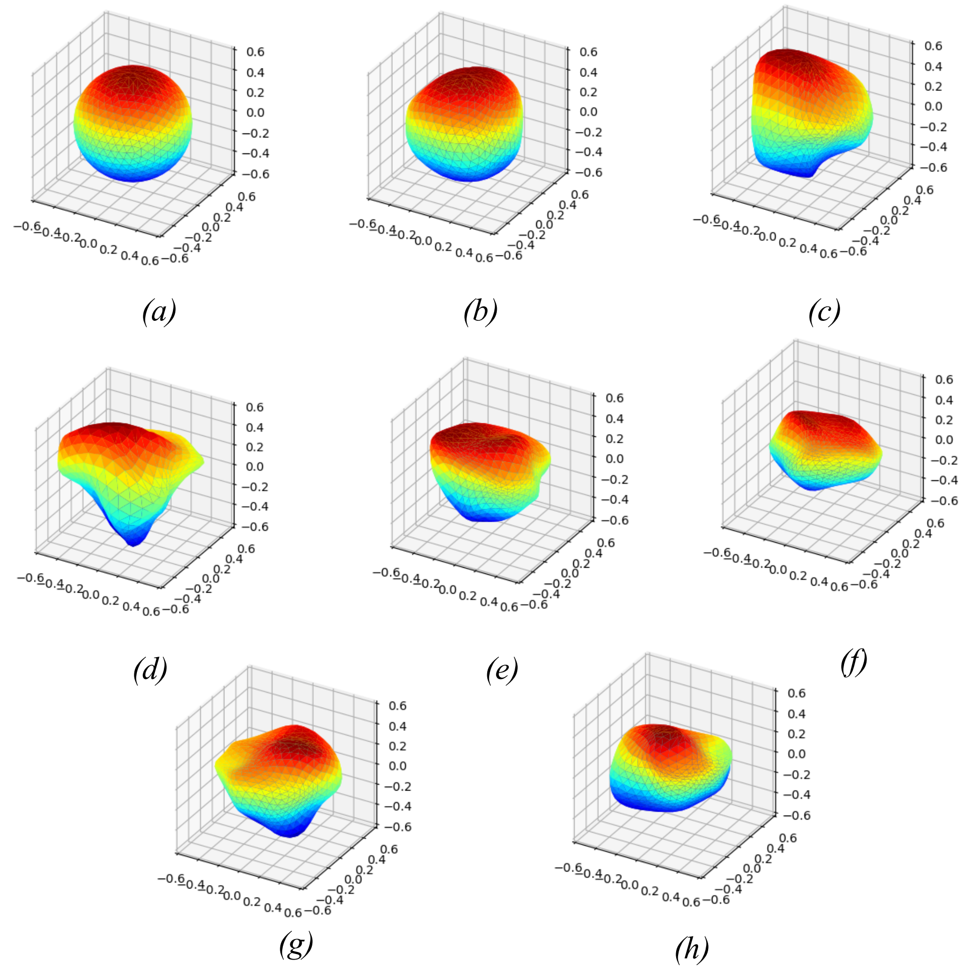

Various particle shapes using the spherical harmonics method ($d_{2\text{-}8}$/EI/FI)
(a-d) 0-0.6/1/1 (e-f) 0.4/0.8,0.6/1 (g-h) 0.4/1/0.8,0.6
**The jet scale indicates the latitude of the particles*

***D. Wei et al., Powder Technology 330 (2018), p.284*

Geometrical feature extraction

- variational auto-encoder：
  - the encoder and the decoder.

The encoder can be used to reduce the high dimensional geometries into a lower-order feature vectors, which can in turn be used to recover the geometry.

$$
\begin{aligned}
&Loss(\boldsymbol{x}^{(i)}) \\
&= -D_{KL}(q_\theta(\mathbf{z}|\boldsymbol{x}^{(i)})||p(\mathbf{z})) \\
&+ E_{q_\theta(\mathbf{z}|\boldsymbol{x}^{(i)})}[\log p_\phi(\boldsymbol{x}^{(i)}|\mathbf{z})] \\
&+ \lambda \sum_{i=1}^{N} (f - f_i)^2
\end{aligned}
$$

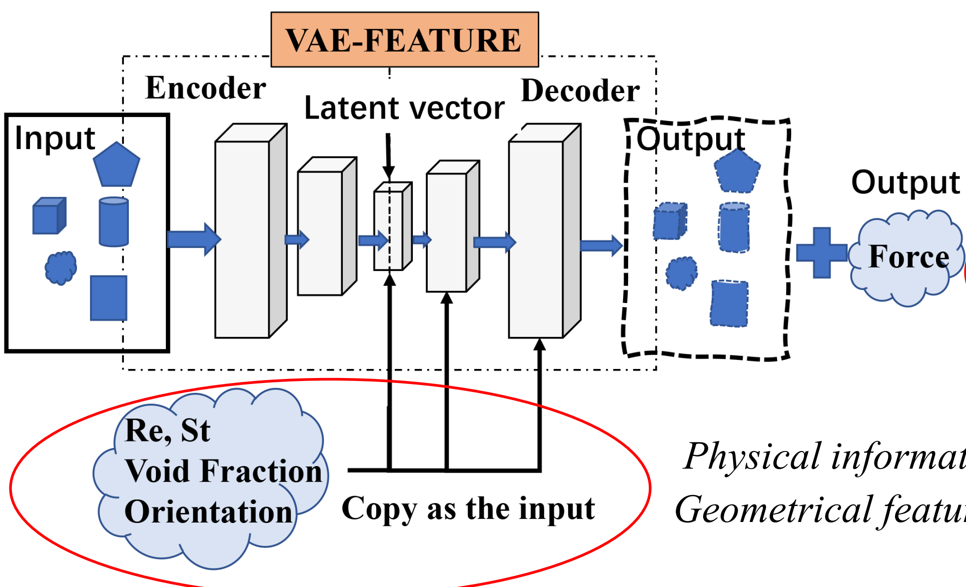

Physical information fed in
Geometrical feature is physically meaningful

MLP for regression

- Multi-layer perceptron will be concatenated after the encoder of VAE-FEATURE

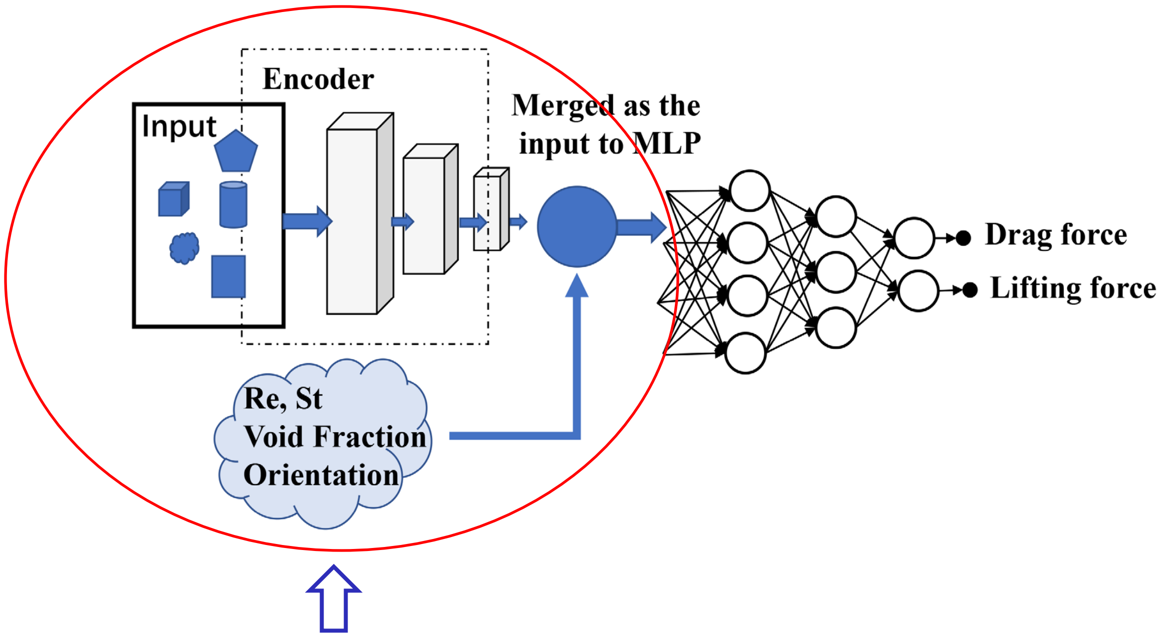

Unchanged or minor adjustment adjointly.

Tasks for the proposed work

	Tasks	Year1				Year2				Year3			
		Q1	Q2	Q3	Q4	Q1	Q2	Q3	Q4	Q1	Q2	Q3	Q4
1	**Project Management and Planning**												
2	**Developing Code for Non-spherical Particles.**												
2.1	*Coupling the non-spherical particle-particle collision module.*												
2.2	*Efficiency improvement of the code.*												
	Milestone A. Code acceleration and verification for non-spherical particles completed		▲										
	Decision Point 1: Validation of highly efficient simulation for gas-particle systems with non-spherical particles		●										
3	**Geometric Database for Non-spherical Particles.**												
3.1	*Collecting 3-D Shapes of Particles*												
3.2	*Generation of Diverse Non-spherical Shapes.*												
3.3	*Generation of Lagrangian Markers.*												
	Milestone B. Generative model for Non-spherical particle shape libraries completed				▲								
4	**Data collection by PR-DNS Method.**												
4.1	*Simulation in Low-Reynolds Numbers.*												
	Milestone C. Database for Gas-solid flows of non-spherical particles in low Reynolds numbers constructed						▲						
4.2	*Simulation in Moderate-Reynolds Numbers.*												
	MileStone E. Database for Gas-solid flows of non-spherical particles in moderate Reynolds numbers constructed											▲	
	Decision Point 3. Validation of MLP Architecture for interaction force model in moderate Reynolds number											●	
5	**Extracting Geometrical Features.**												
5.1	*Construction of the VAE architecture.*												
5.2	*Training, validation and Optimization of the VAE model.*												
6	**Training of MLP-based Regressor and Final Reporting.**												
6.1	*Construction of the MLP architecture.*												
	Milestone D: Interaction force model for non-spherical particles in low Reynolds number completed								▲				
	Decision Point 2. Validation of MLP Architecture for interaction force model in low Reynolds number								●				
6.2	*Training, Validation and Optimization of MLP.*												
6.3	*Linking of the model to MFiX and Final Reporting.*												
	Milestone F: Training and verification of interaction force model and Likning to MFiX												▲